

DTP/96/76  
UR-1473  
ILL-(TH)-96-8  
hep-ph/9609246  
August 1996

# Gluon Radiation in $t\bar{t}$ Production and Decay at the LHC

Lynne H. Orr

*Department of Physics, University of Rochester  
Rochester, NY 14627-0171, USA*

T. Stelzer

*Department of Physics, University of Illinois-Urbana  
Urbana, Illinois 61801, USA*

and

W.J. Stirling

*Departments of Physics and Mathematical Sciences, University of Durham  
Durham DH1 3LE, England*

## Abstract

Understanding the pattern of gluon radiation in  $t\bar{t}$  production and decay processes is important for making an accurate determination of the top mass from the momenta of its decay products. The larger energy of the LHC  $pp$  collider boosts the top cross section by a factor of 100 compared to that at the Tevatron, but it also increases the amount of additional gluon radiation. We calculate the cross section for gluon radiation in top production and decay at the LHC. The distributions of this radiation are presented and the exact matrix-element results are compared with results from the HERWIG parton-shower Monte Carlo.

# 1 Introduction

Reconstructing the top mass is critical to many of the physics goals of the LHC. The top-quark mass is interesting in its own right as a fundamental parameter of the standard model (SM), and for its role in pinning down other aspects of the SM and its extensions. Our ability to reconstruct  $m_t$  also affects new physics search strategies, in which top can appear as a signal or background. Reconstructing the top mass on an event by event basis is an important tool for distinguishing top production from other processes. Estimates for future runs at the Tevatron, extrapolated from early Run 1 results, suggest that  $m_t$  will be measured at the 4 GeV level [1]. Recent improvements in Tevatron results [2] may lead to more optimistic conclusions. At the LHC, given the enhanced statistics, experiments may hope for an accuracy of 2 GeV [3]. But the ability to do this will depend on how well systematic effects — especially those associated with gluon radiation — are understood and controlled. It is therefore crucial to properly simulate the relevant physics.

By virtue of its energy and luminosity, the LHC will be a top factory. The top cross section at the 14 TeV LHC is more than 100 times larger than at the 2 TeV Tevatron. This increase in production rate has a price, however: an increase in gluon radiation. In a  $t\bar{t}$  interaction, 7 TeV protons can easily radiate quarks and gluons with only a small penalty to be paid in the parton distributions. As a result, at the LHC there will be a plethora of radiation associated with top pair production. This radiation may well be the limiting factor in our ability to reconstruct the top mass, both on an event by event basis, and from global shapes. For example, the sheer quantity of radiation could result in emissions associated with top production (as opposed to decay) being included in the  $b$ -quark jet cone, introducing spurious contributions to the top mass reconstruction. Additional jets may also introduce difficulties in choosing the appropriate jets for reconstructing momenta in the lepton+jets channel.

This paper is an investigation of the effects of gluon radiation in top events at the LHC. In the next section, we compare  $t\bar{t}$  and  $t\bar{t}g$  production at the LHC to that at the Tevatron. We then present in Section 3 a complete tree-level  $\alpha_s^3$  calculation of  $pp \rightarrow W^+W^-b\bar{b}j$ . We present distributions of the radiated jets, with the radiation decomposed into production- and decay-stage emission. In Section 4 we compare our matrix element results with those from the parton shower Monte Carlo HERWIG, and we comment on the precision to which HERWIG appears to have this physics implemented for gluon radiation in top-quark production and decay. In Section 5 we present our conclusions.

## 2 $t\bar{t}$ and $t\bar{t}g$ production at the Tevatron and LHC

To understand the effects of gluon radiation in top events at the LHC, it is useful to compare top production there and at the Tevatron. The most obvious difference is in the  $t\bar{t}$  production cross section, which is on the order of 100 times higher at the LHC. More relevant for our purposes is a similarity between the two machines: the fact that for heavy quark production, the mass of the quark rather than the collider energy sets the scale for the quark's transverse momentum. This is illustrated in Figure 1, which shows the transverse momentum of top quarks produced at the Tevatron<sup>1</sup> (solid line) and LHC (dashed line), normalized to the Tevatron cross section. Despite the factor of seven difference in collider energy, the transverse momentum of the top quarks at the two machines is remarkably similar. The only noticeable effect of the LHC's higher energy is a slight spread in the distribution at larger  $p_T$ . (And although we do not show it here, top quarks are produced at the LHC with broader rapidity distributions.) Similar results are seen for  $t\bar{t}j$  production.

This similarity in top quark spectra at the two machines has several consequences. The most notable is the set of  $x$  values at which the parton distributions of the proton are probed at the two machines. At the Tevatron, the parton typically has a fraction  $x \simeq 0.2$  of the proton's energy. At the LHC, the typical value is only  $x \simeq 0.03$ . This results in 90% of the top quarks produced at the Tevatron coming from  $q\bar{q}$  annihilation, whereas at the LHC about 90% of the top quarks come from the  $gg$  initial state. This means, among other things, that we expect more gluon radiation in top production at the LHC because of the gluons' larger color charge. A second consequence of the similarity in top quark spectra is that gluon emission in top quark *decay* at the LHC should be similar to that at the Tevatron. At the LHC, therefore, gluon radiation is dominated by production-stage emission.

We will discuss the full gluon distributions below, but because of the production-stage dominance we can draw a few general conclusions about the importance of radiation in top events by considering  $t\bar{t}j$  production.<sup>2</sup> Figure 2 shows the ratio of cross sections for  $t\bar{t}g$  and  $t\bar{t}$  production at the Tevatron (solid line) and LHC (dashed line) as a function of the minimum transverse energy  $E_T$  of the gluon. The great enhancement for production stage emission at the LHC can be attributed to two sources. First, as mentioned above, gluons carry a larger color charge than quarks. Therefore the color in the  $gg$  initial state at the LHC enhances gluon emission by a factor of approximately  $C_A/C_F = 9/4$  over the  $q\bar{q}$  initial state at the Tevatron.

---

<sup>1</sup>With center-of-mass energy 1.8 TeV

<sup>2</sup>In this calculation and in those below, we have chosen the strong coupling constant scale as follows. The factors of  $\alpha_s$  associated with the lowest-order part of each process are evaluated at  $\sqrt{\hat{s}}$ , the total subprocess center-of-mass energy. The additional factor of  $\alpha_s$  associated with emission of the extra jet is evaluated at the jet's transverse energy  $E_{Tj}$ . Thus each  $t\bar{t}j$  cross section contains an overall factor  $\alpha_s^2(\sqrt{\hat{s}})\alpha_s(E_{Tj})$ .

Second, the parton distributions at the Tevatron fall very steeply in the relevant  $x$  range, making it difficult to provide the additional energy required for a production stage emission. At the LHC, the additional energy can be obtained with less of a cost in the parton densities.

These effects are illustrated in the table, where we compare the contributions to  $t\bar{t}$  and  $t\bar{t}j$  production at the Tevatron and LHC. Cross sections are given in picobarns with cuts on the extra jet as indicated. If we compare the ratios  $\sigma(t\bar{t}j)/\sigma(t\bar{t})$  for the  $q\bar{q}$  and  $gg$  initial states, we see an enhancement for  $gg$  compared to  $q\bar{q}$ , as we would expect due to the larger color factor in the  $gg$  initial state. This happens for both colliders. A closer look shows that the  $gg$  enhancement is larger at the LHC, where we have, for  $E_{Tj} > 40$  GeV,  $\sigma(gg \rightarrow t\bar{t}g)/\sigma(gg \rightarrow t\bar{t}) = 0.46$  and  $\sigma(q\bar{q} \rightarrow t\bar{t}g)/\sigma(q\bar{q} \rightarrow t\bar{t}) = 0.16$ . At the Tevatron, these ratios are, respectively, 0.1 and 0.07. The larger increase in the  $gg$  cross section over  $q\bar{q}$  at the LHC is due to the difference in behavior of the parton distributions discussed above.

		$q\bar{q}$	$gg$	$qg, \bar{q}g$
Tevatron	$t\bar{t}$	2.4	0.2	-
	$t\bar{t}j, E_{Tj} > 10$ GeV	1.1	0.2	0.1
	$t\bar{t}j, E_{Tj} > 40$ GeV	0.17	0.02	0.03
LHC	$t\bar{t}$	50	330	-
	$t\bar{t}j, E_{Tj} > 10$ GeV	35	590	146
	$t\bar{t}j, E_{Tj} > 40$ GeV	8	151	63

Although Fig. 2 provides an indication of the relative importance of gluon radiation at the Tevatron and LHC, it should not be taken too literally. For example, it should not be translated directly into an expected number of top events containing an extra gluon. There are several reasons for this. First, only production-stage radiation is explicitly included. Second, and more important, it represents a fixed-order matrix element calculation which includes neither virtual effects nor effects due to multiple gluon emission, both of which can be important for low gluon energies.

In fact the figure serves as a guide to the regions where we can and cannot trust the matrix-element results. Roughly speaking, they are reliable when the  $t\bar{t}g$  cross section is well below  $\sigma(t\bar{t})$ . This is satisfied at the Tevatron for all  $E_T$  cuts shown. At the LHC, however, the first-order cross section rises dramatically with decreasing  $E_T$  cut, and the  $t\bar{t}g$  cross section with gluon transverse energies greater than 10 GeV exceeds the lowest-order cross section by a factor of 2, as can be seen in Fig. 2 and the table. Clearly virtual and multi-gluon effects must be important there. We therefore restrict our LHC analysis to gluons with transverse momentum greater than 40 GeV in what follows.

### 3 Gluon radiation in top production and decay

It is useful to distinguish between two different types of radiation in  $t\bar{t}$  processes, as we have implicitly done above and as has been discussed in previous work [4, 5, 6]. Gluons can be radiated in either the top production or decay stages. Production-stage emission occurs before the top quark goes on shell and decay-stage emission occurs only after the top quark goes on shell. In principle, an event with an extra jet can be classified as ‘production’ or ‘decay’ by looking at the invariant mass of the decay products. In production emission events, the  $W$  and  $b$  momenta will combine to give the top momenta. In decay emission events, the gluon momentum must also be included to reconstruct the top momenta.

This interpretation is exact at the parton level in the narrow width approximation. Finite top width effects can blur this interpretation due to interferences between production-and decay-stage emissions. However, the classification is still useful in our case because the top width of 1.5 GeV is small compared to the 40 GeV gluon  $E_T$  cut imposed in the matrix element calculations. It should be kept in mind that this applies at the level of theory. In an experiment, the production-decay distinction is further blurred by jet energy resolution and ambiguities associated with combinatorics and the like.

We have performed a complete tree-level  $O(\alpha_s^3)$  calculation of  $pp \rightarrow W^+W^-b\bar{b}j$  at 14 TeV collision energy. The calculation was performed as in [6], with the exception of the choice of  $\alpha_s$  scale as discussed above. We include all contributing diagrams<sup>3</sup> and their interferences (with helicity amplitudes generated by MadGraph [7]), and all top width and  $b$  mass effects. Note that we do *not* include radiation off the  $W$  decay products. We use MRS(A') parton distributions [8]. The kinematic cuts imposed on the final-state partons are (the subscript  $j$  refers to the extra jet only):<sup>4</sup>

$$\begin{aligned}
 |\eta_j| &\leq 3, \\
 |\eta_b| &\leq 2, \\
 E_{Tj}, &\geq 40 \text{ GeV}, \\
 E_{Tb}, &\geq 20 \text{ GeV}, \\
 \Delta R_{bj}, \Delta R_{b\bar{b}} &\geq 0.4.
 \end{aligned}
 \tag{1}$$

The resulting distributions for the extra jet at the LHC are shown in Figures 3–5. In each figure the distribution is decomposed into contributions from production- (dashed line) and decay-stage (solid line) radiation according to final-state kinematics as described in [6]. The most obvious feature of these distributions is the dominance

---

<sup>3</sup>We include all processes that give rise to an extra jet:  $q\bar{q} \rightarrow b\bar{b}W^+W^-g$ ,  $gg \rightarrow b\bar{b}W^+W^-g$ , and  $gg(\bar{q}q) \rightarrow b\bar{b}W^+W^-q(\bar{q})$ .

<sup>4</sup>The cuts are applied to both the  $b$  and  $\bar{b}$  quarks.

of production over decay emission, due to the enhancements in production emission discussed above. The decay contribution does not receive this enhancement because its behavior is determined not by the collider energy, but by the phase space of a 175 GeV top-quark decay.

In addition to the relative size, the kinematics of the two types of emission are also interesting. Figure 3 shows the jet  $E_T$  distribution. Both contributions fall off with increasing  $E_T$ , but production emission extends to much higher values. The smaller values of  $E_T$  to which decay emission is constrained are again the consequence of the top decay kinematics. Recall that even at the LHC, top quarks are produced with relatively modest transverse momentum (cf. Fig. 1), so that gluons from the decay do not receive much of a boost in  $E_t$ . Note also that an increase in the  $E_T$  cut on the jet would result in a further reduction in relative size of the decay contribution compared to production.

Figure 4 shows the distribution in pseudorapidity of the extra jet. Production emission is relatively flat in rapidity, as compared to the more central decay emission. This is consistent with our basic intuition that decay-stage radiation, being associated with the final-state particles — which tend to appear in the central rapidity region — is also likely to be produced centrally. But this decay contribution is small; the important point to note here is that even in the central region, it is production-stage radiation that dominates.

The tendency of decay-stage radiation to be associated with the final-state  $b$  quarks might lead one to expect that if the extra jet is ‘near’ the  $b$  jet it should be included in the mass reconstruction, and if it is not it should be excluded. Figure 5, which shows the distribution in  $\Delta R$  between the jet and the nearest  $b$  quark, confirms that the decay-stage radiation peaks close to the  $b$  and production-stage radiation peaks further away. Unfortunately, the production contribution is so large that it dominates even at the low  $\Delta R$  cutoff. A higher  $E_T$  cut on the jet would make this situation even worse. The best choice of what is ‘near’ the  $b$  quark will therefore balance the competing effects of decay emission falling outside the cone, and production emission falling inside the cone.

It is tempting at this point to provide a prescription for dealing with the extra jets expected in top events at the LHC, for example by specifying how to make the best choice of what is ‘near’ the  $b$  quark. But optimizing this choice at the parton level would be naive, because effects of multiple emissions, hadronization, and detector resolution will all affect the results.

We also note that radiation from  $W$  decay products has not been included in our analysis here. Since the best top mass reconstruction is obtained in the lepton+jets mode, radiation from hadronic  $W$  decays must ultimately be included. This calculation has been done in the soft gluon approximation [5], and the contribution from a single hadronically decaying  $W$  is found to be substantial — comparable in size and shape

to the *total* decay contributions from radiation off the  $tb$  and  $t\bar{b}$  antennae. The exact calculation including hadronic  $W$  decays is currently in progress [9].

In practice the effects of gluon radiation are incorporated into the predictions that are used in experimental fits. The parton level calculation can and should be used to ensure that the radiation physics is properly implemented in event generators used in the experimental analysis.

## 4 Comparison with HERWIG

Because the experimental analysis must rely on the predictions of Monte Carlo programs — for example, in fits to three-jet invariant mass distributions for top mass determination — it is important that these programs contain the correct physics. The Monte Carlo program HERWIG [10], which is widely used in experimental analyses, treats gluon radiation in top production and decay using parton showers.

In previous work [6, 11], we compared our results for radiation at the Tevatron with predictions of version 5.8 of HERWIG. We found significant discrepancies in regions where the two should agree. HERWIG appeared to have a deficit in decay-stage radiation compared to production [6]. Further investigation revealed differences even for  $t\bar{t}g$  production at  $e^+e^-$  colliders [11]. Recently HERWIG 5.8 was found to contain a bug [13, 14] which resulted in suppression of decay-stage radiation in top events.<sup>5</sup> Here we continue our comparison of matrix-element and parton-shower results using HERWIG 5.9 [14], in which the bug has been corrected. Although we see some improvement in the agreement, major differences still exist.

We begin by reproducing the LHC jet distributions using HERWIG 5.9. The details of comparing a full parton shower Monte Carlo with a fixed-order matrix element calculation were discussed in previous papers [6, 11]. The idea is to combine particles from the parton shower into jets, and compare distributions of these jets to those from the matrix element calculation. For hadron colliders we use a cone algorithm to combine partons into jets. We identify events with production- and decay-stage emission according to the final state kinematics, as described above.

Results for the jet pseudorapidity are shown in Figure 6. There is general agreement between the matrix element calculation and the parton shower. However, a closer examination reveals two important differences. Looking at production emission, we see that the HERWIG distribution is peaked at large  $|\eta|$  and has a dip in the center. In contrast, the matrix element distribution is relatively flat, as we have seen in Fig. 4. Since the jets in this case have relatively strong cuts, the perturbation series should be converging quickly and the tree-level matrix element distributions should be accurate. This suggests that the approximations used in HERWIG may be responsible for this discrepancy.

---

<sup>5</sup>The bug appeared only in version 5.8; it was not present in HERWIG 5.7 [14].

The second difference between the matrix-element and parton-shower results is, as before, in the relative amounts of production and decay emissions. Whereas HERWIG 5.8 with the bug had too *little* decay-stage radiation, the corrected version now seems to have too *much* compared to the matrix element calculation.

This effect is illustrated more clearly in a simpler example. As in our previous work [11], we simplify the comparison by looking at  $e^+e^-$  machines near  $t\bar{t}$  threshold. While the parton calculation is an inclusive calculation with a fixed number of final state particles, HERWIG is an exclusive calculation with an arbitrary number of final particles. To perform a meaningful comparison we employ the Durham ( $k_T$ ) successive recombination algorithm to reconstruct jets from the HERWIG output [12]. In addition, we impose cuts ( $E_{Tj} > 10$  GeV,  $\Delta R > 0.4$ ) on the jets to ensure the matrix element is being evaluated in a region where the perturbation series converges rapidly. The validity of this comparison was demonstrated in [11].

The results of our comparison for  $e^+e^- \rightarrow W^+W^-b\bar{b}g$  are shown in Figure 7, where along with the matrix-element calculation we show results from both the old (5.8) and corrected (5.9) versions of HERWIG. The center-of-mass energy of 360 GeV is chosen just above  $t\bar{t}$  threshold to suppress production-stage emission, so that almost all of the radiation occurs in the decays. Fig. 7(a) shows the distribution in  $\Delta R$  between the closest two jets, and Fig. 7(b) shows the minimum  $y$  (defined in the Durham algorithm as  $y_{ij} \equiv 2 \min(E_i^2, E_j^2)(1 - \cos \theta_{ij})/s$ ) for all jet pairings in the event. We see in both cases that the old version of HERWIG underestimates the amount of decay radiation and the new version vastly overestimates it. The discrepancy even in the corrected version of HERWIG is dramatic.

As a technical aside, we note that the normalization of the matrix element for the  $e^+e^-$  case is fixed as in our previous work [11] by choosing the value of  $\alpha_s = 0.126$  that gives agreement between the matrix-element and parton-shower calculations for the case of  $b\bar{b}$  production. The larger energy scale for top quark production might suggest the use of a smaller value of  $\alpha_s$ , which would make the discrepancy even larger.

The disagreement between the matrix element calculation and HERWIG seems severe. A detailed study of the discrepancy is in progress and will appear elsewhere [9]. For the moment, it appears that an estimate of the magnitude of the effect is the best that can be hoped for. We would expect this effect to contribute on the order of a few GeV to the uncertainty in the measured top mass. While not catastrophic, clearly such a discrepancy is unacceptably large, given the precision hoped for in future experiments. Further work must be done to provide an accurate event generator for top-quark production.

## 5 Conclusions

Top-quark production will be central to many physics studies at the LHC, and top mass reconstruction will be the key for identifying top events. The large energy of the LHC collider provides a large top-quark cross section, but it also provides for large amounts of gluon radiation in the top production process. We have calculated the cross section for top production and decay in association with an extra jet to order  $\alpha_s^3$ , and find a large probability for gluon radiation at the LHC compared to the Tevatron. At the LHC, production-stage radiation dominates over decay-stage emissions; this is also in contrast to the Tevatron, where the two contributions are roughly comparable. As shown above, the relative amounts of production- and decay-stage radiation depend sensitively on the kinematic cuts applied. In addition, the decay contribution is expected roughly to double if radiation from hadronic  $W$  decays is included.

All of this has important implications for top physics at the LHC. Even more so than at the Tevatron, gluon radiation at the LHC must be understood not only because there is more of it, but because uncertainties in quantities like the top mass will be dominated by systematic effects due to gluon radiation. For example, the proliferation of production-stage gluon radiation means that it will sometimes be included in the top mass reconstruction, and therefore will limit our ability to reconstruct the top mass. Quantifying the magnitude of this and similar effects requires simulations which implement all of the relevant physics correctly. Unfortunately our comparisons show that even the most recent version of HERWIG, corrected for the bug in version 5.8, still does not reproduce the correct distributions. Apparently a hard gluon correction is needed to model radiation in the production and decay of very heavy quarks. It should be a priority to provide a top-quark event generator with the standard model physics implemented as accurately as possible.

## Acknowledgements

WJS is grateful to the UK PPARC for a Senior Fellowship. Useful discussions with Tony Liss, Richard Partridge and Paul Tipton are acknowledged. This work was supported in part by the U.S. Department of Energy, under grant DE-FG02-91ER40685 and by the EU Programme “Human Capital and Mobility”, Network “Physics at High Energy Colliders”, contract CHRX-CT93-0537 (DG 12 COMA).

## References

- [1] TeV-2000 study group, D. Amidei *et al.*, FERMILAB-PUB-96-082, April 1996.

- [2] P. Tipton, presented at the XXVIII International Conference on High Energy Physics, Warsaw, Poland, July 1996.
- [3] ATLAS Technical Proposal, CERN/LHCC 94-43, LHCC/P2, 1994; CMS Technical Proposal, CERN/LHCC 94-38, LHCC/P1, 1994.
- [4] V.A. Khoze, L.H. Orr and W.J. Stirling, Nucl. Phys. **B378** (1992) 413; V.A. Khoze, J. Ohnemus and W.J. Stirling, Phys. Rev. **D49** (1994) 1237; L.H. Orr and W.J. Stirling, Phys. Rev. **D51** (1995) 1077.
- [5] B. Masuda, L.H. Orr and W.J. Stirling, preprint UR-1452, Phys. Rev. **D**, in press.
- [6] L.H. Orr, T. Stelzer and W.J. Stirling, Phys. Rev. **D52** (1995) 124.
- [7] T. Stelzer and W.F. Long, Comp. Phys. Commun. **81** (1994) 357.
- [8] A.D. Martin, R.G. Roberts and W.J. Stirling, Phys. Lett. **B354** (1995) 155.
- [9] L.H. Orr, T. Stelzer and W.J. Stirling, in progress.
- [10] G. Marchesini and B.R. Webber, Nucl. Phys. **B310** (1988) 461; G. Marchesini, B.R. Webber, G. Abbiendi, I.G. Knowles, M.H. Seymour and L. Stanco, Comp. Phys. Commun. **67** (1992) 465.
- [11] L.H. Orr, T. Stelzer and W.J. Stirling, Phys. Lett. **B354** (1995) 442.
- [12] S. Catani, Yu.L. Dokshitzer, M. Olsson, G. Turnock and B.R. Webber, Phys. Lett. **B269** (1991) 432.
- [13] S. Snyder, private communication.
- [14] G. Marchesini *et al.*, hep-ph/9607393.

Figure 1

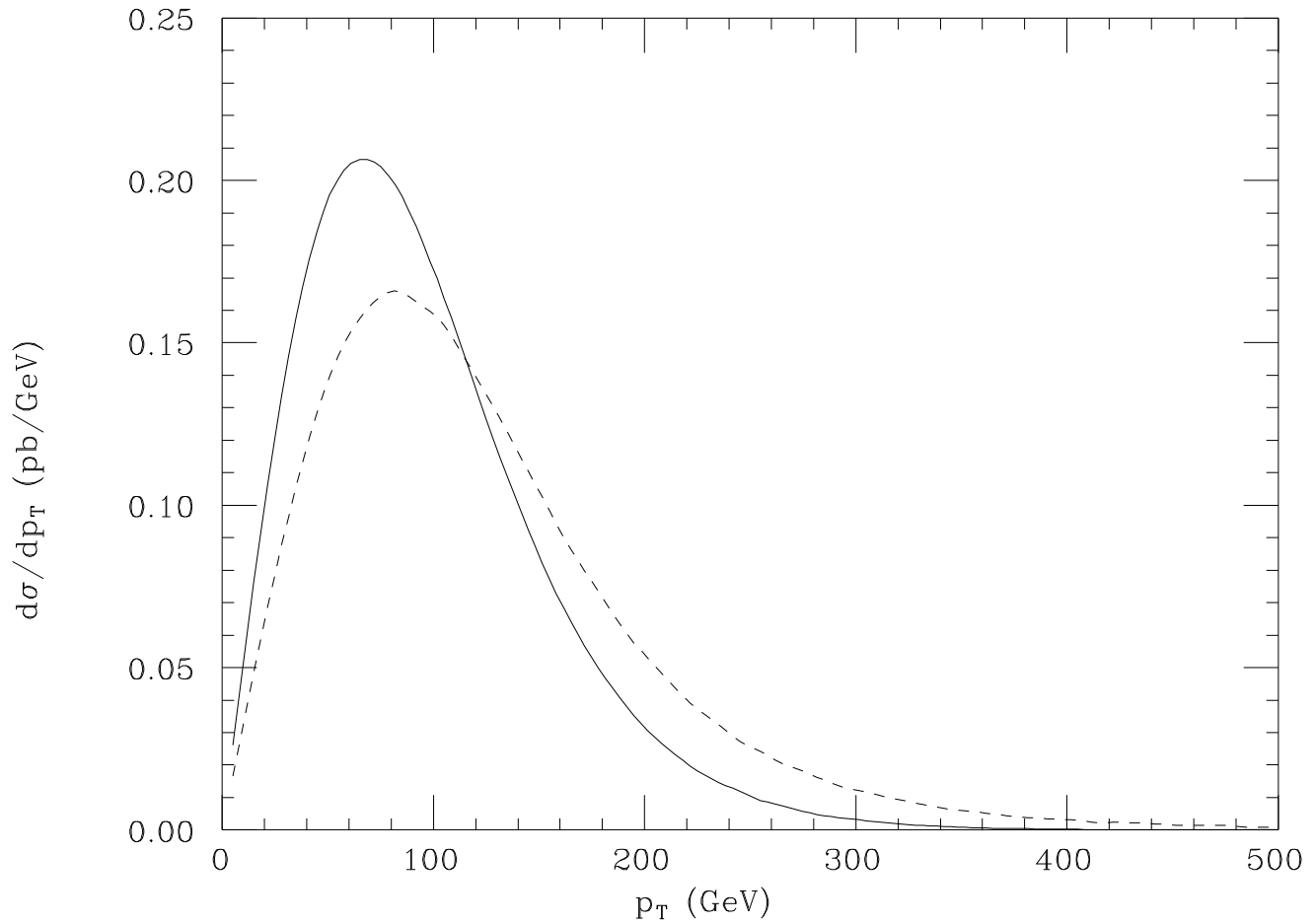


Figure 1: Distribution in top quark transverse momentum for  $t\bar{t}$  production at the Tevatron (solid line) and the LHC (dashed line). The LHC curve is normalized to the total  $t\bar{t}$  cross section at the Tevatron.

Figure 2

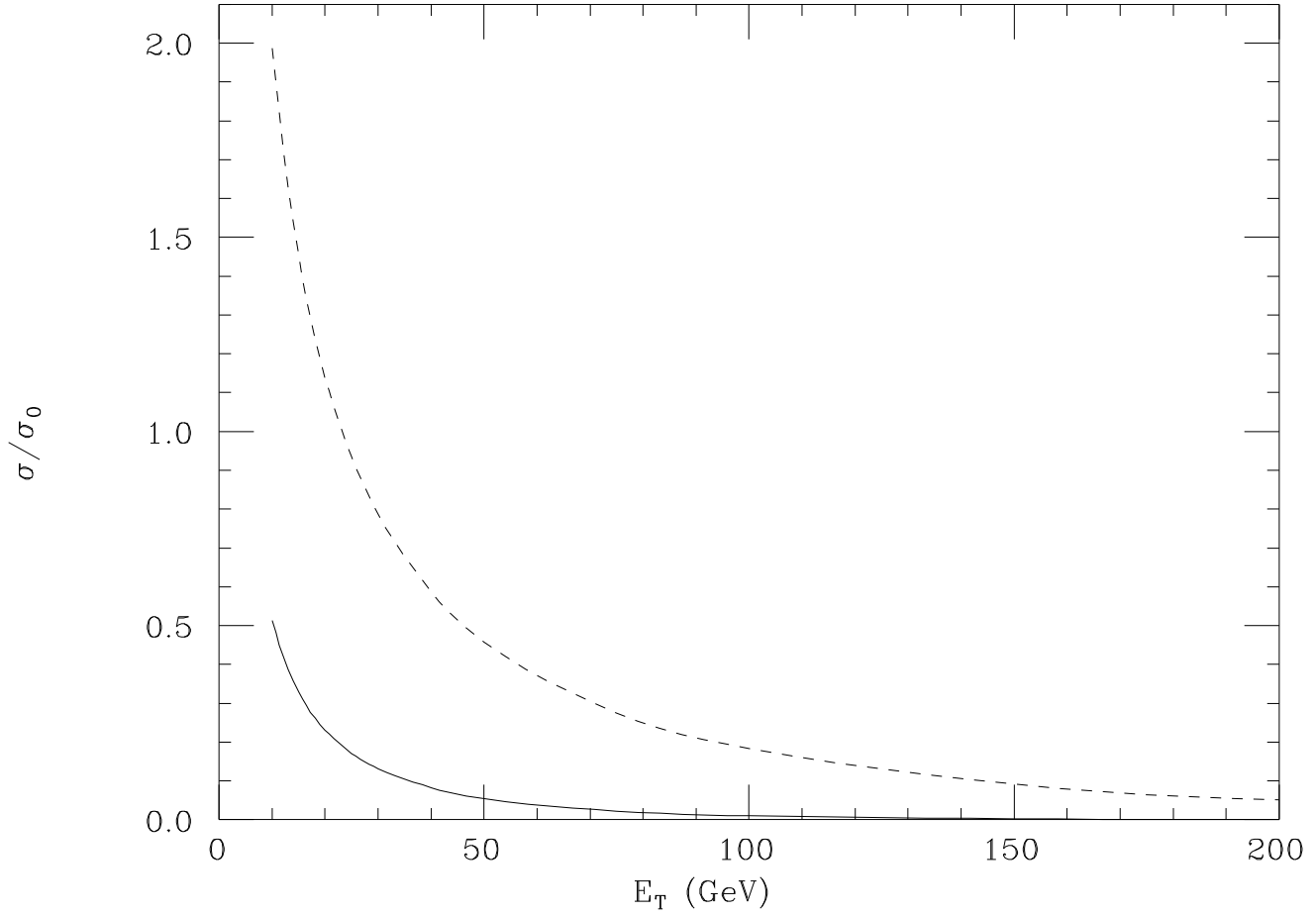


Figure 2: Ratio of  $\sigma(t\bar{t}j)$  to  $\sigma(t\bar{t})$  for  $E_T^j > E_T$  at the Tevatron (solid line) and LHC (dashed line). In both cases  $t\bar{t}j$  production includes the subprocesses  $q\bar{q} \rightarrow t\bar{t}g$ ,  $g\bar{g} \rightarrow t\bar{t}q$ ,  $qg \rightarrow t\bar{t}q$ , and  $\bar{q}g \rightarrow t\bar{t}\bar{q}$ .

Figure 3

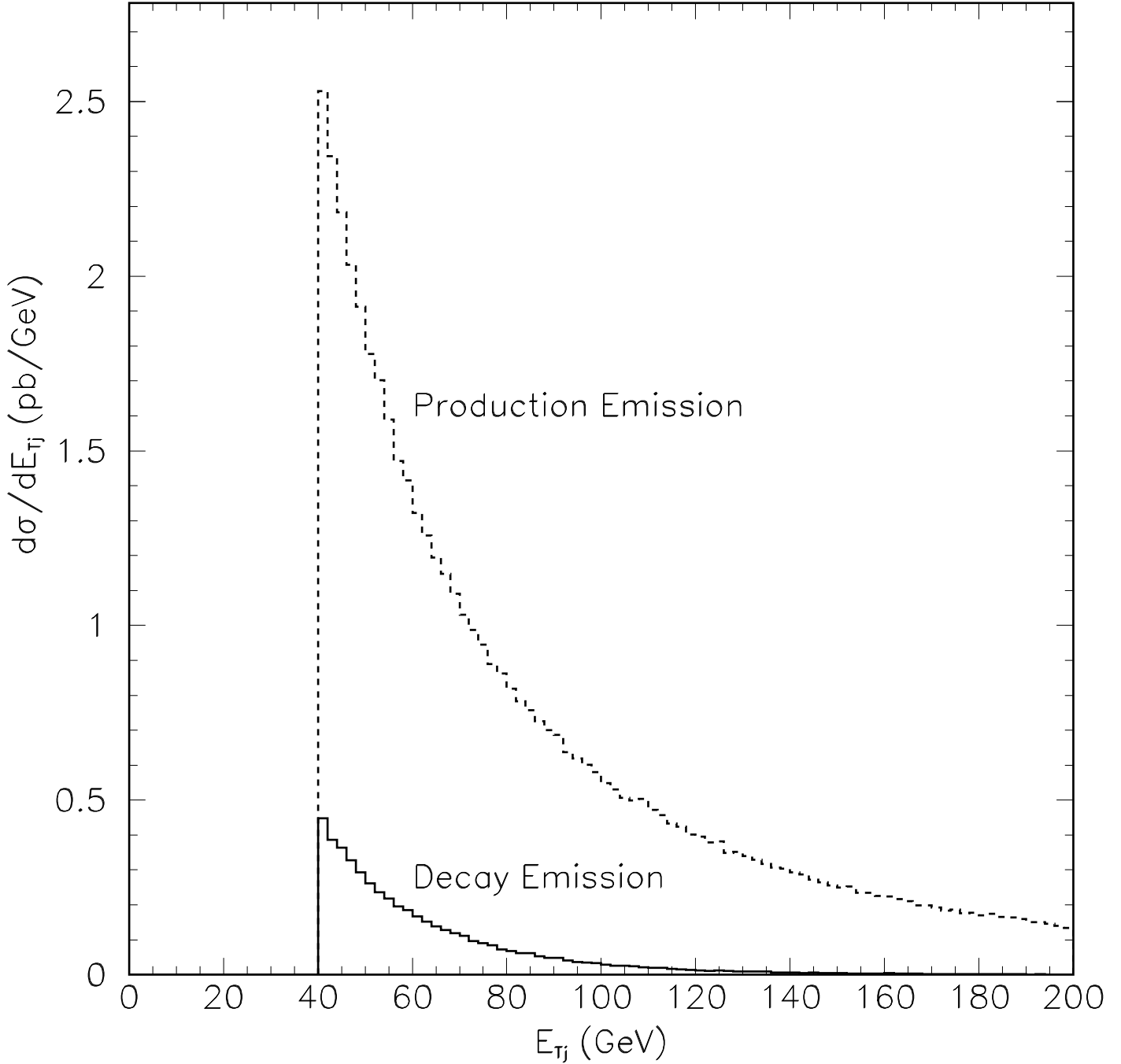


Figure 3: Transverse energy distribution for jets produced in association with top production and decay, via the subprocesses  $q\bar{q}, gg \rightarrow bW^+\bar{b}W^-g$  and  $qg(\bar{q}g) \rightarrow bW^+\bar{b}W^-q(\bar{q})$ , in  $pp$  collisions at  $\sqrt{s} = 14$  TeV. Contributions from production- (dashed histogram), and decay-stage (solid histogram) emissions are shown. The cuts are listed in Eq. (1).

Figure 4

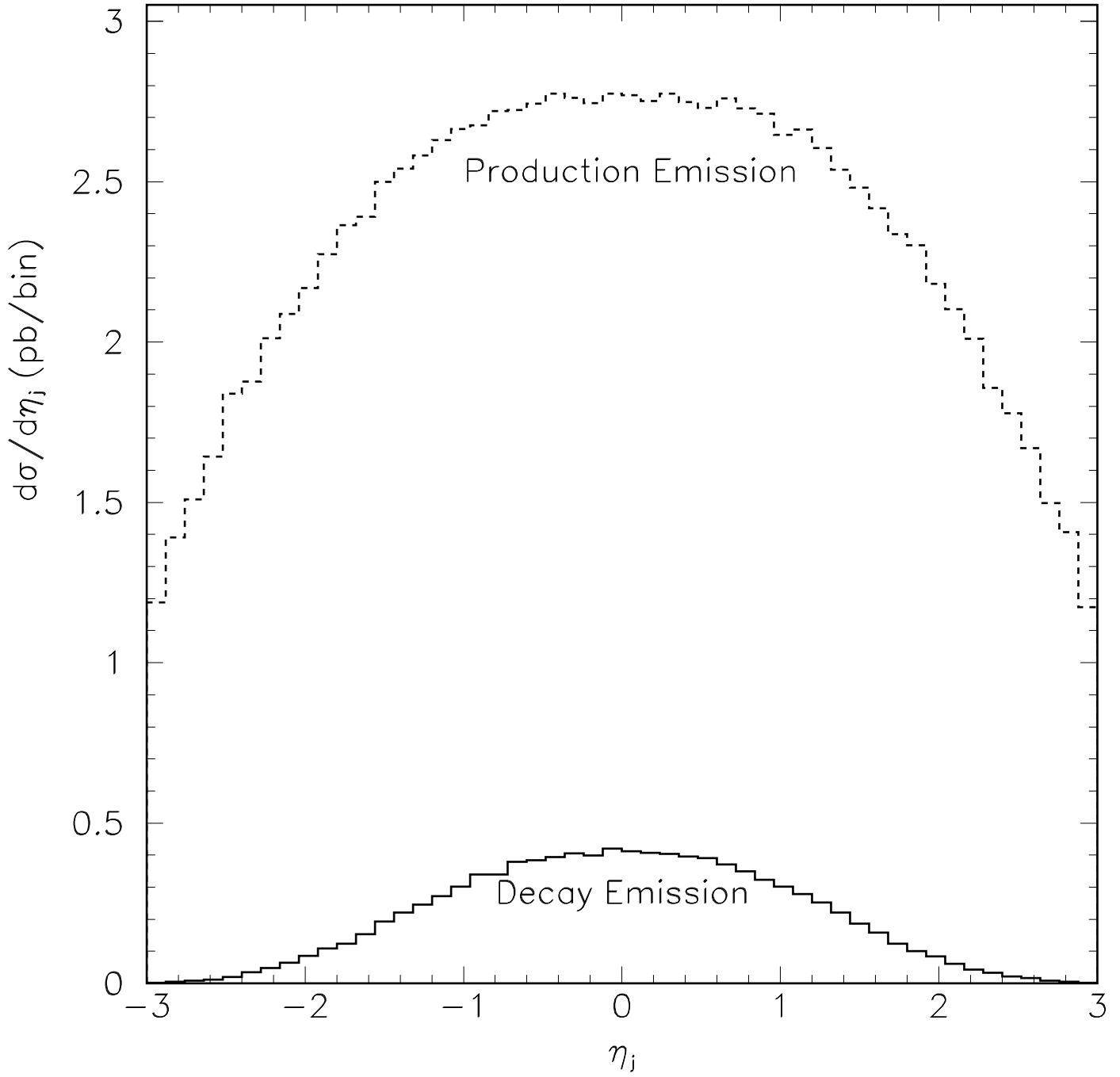


Figure 4: Pseudorapidity distribution for jets produced in association with top production and decay at the LHC. Contributions from production- (dashed histogram), and decay-stage (solid histogram) emissions are shown. The cuts are listed in Eq. (1).

Figure 5

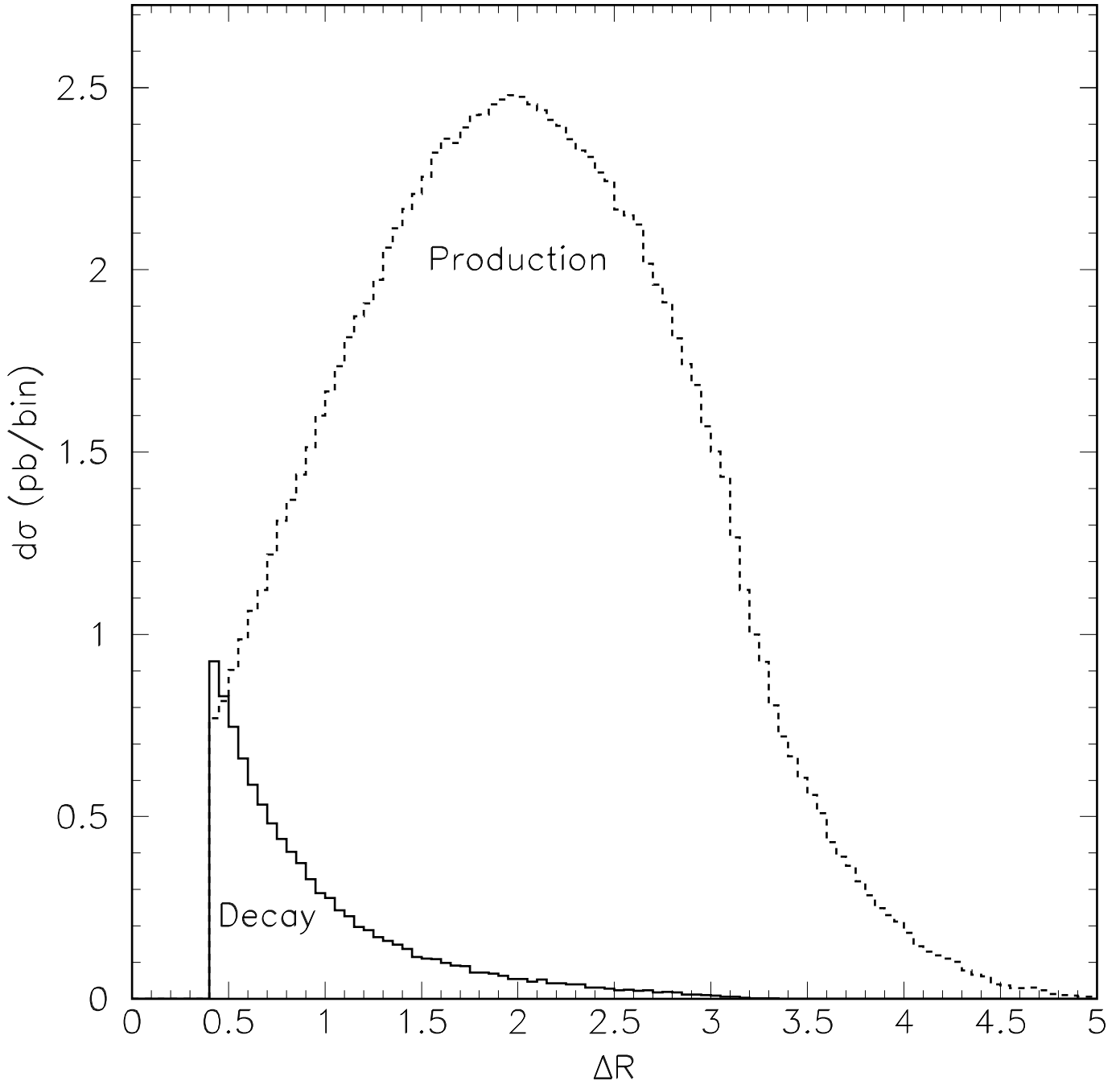


Figure 5: Distribution in the jet- $b$  angular separation ( $\Delta R_{bj} = (\Delta\eta_{bj}^2 + \Delta\phi_{bj}^2)^{1/2}$ ) for jets produced in association with top production and decay at the LHC. Contributions from production- (dashed histogram), and decay-stage (solid histogram) emissions are shown. The cuts are listed in Eq. (1).

Figure 6

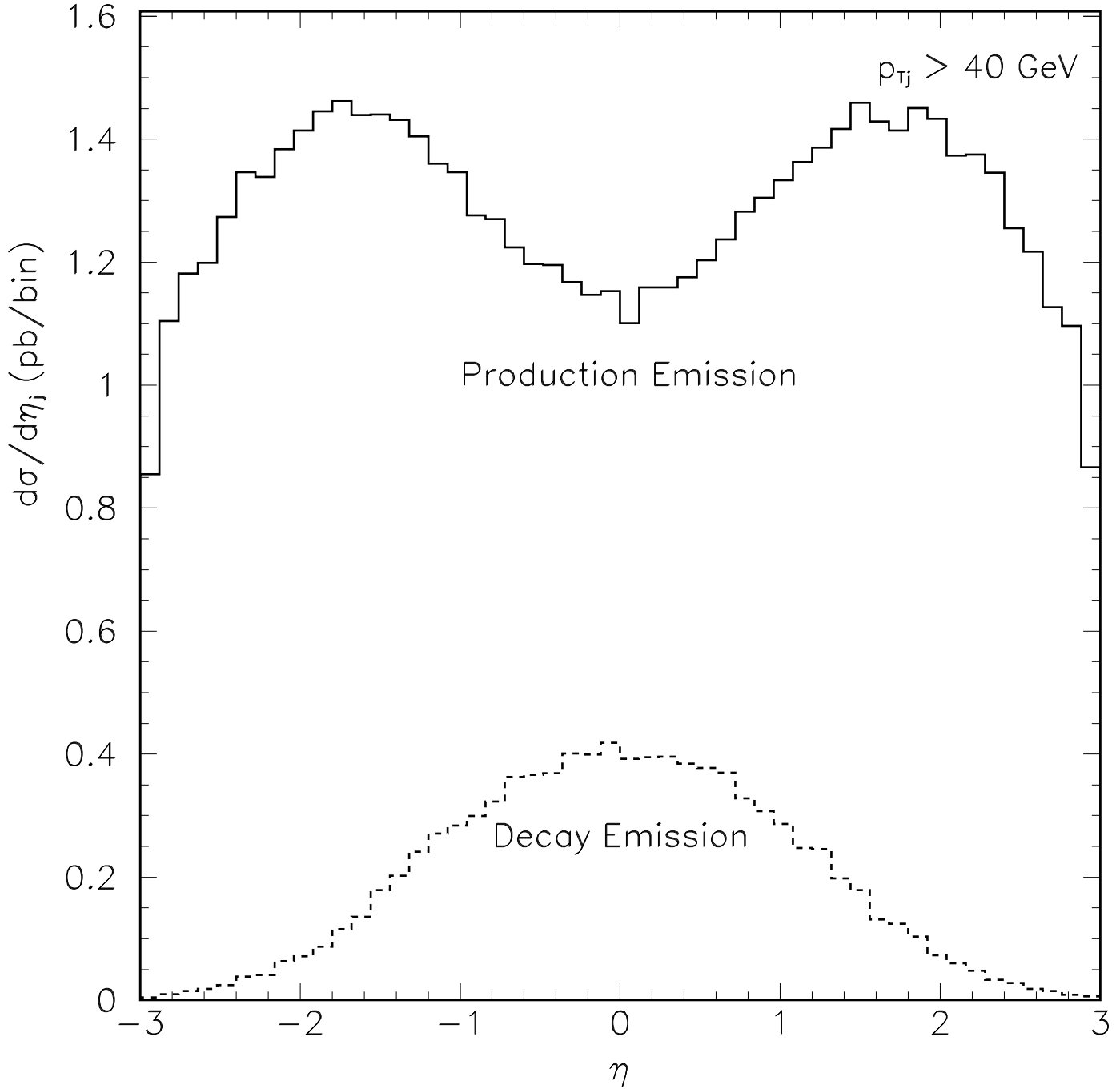


Figure 6: Jet pseudorapidity distribution for extra jets in top production and decay at the LHC as obtained using the HERWIG parton-shower Monte Carlo program, version 5.9. Contributions from production- (dashed histogram), and decay-stage (solid histogram) emissions are shown. The cuts are listed in Eq. (1).

Figure 7

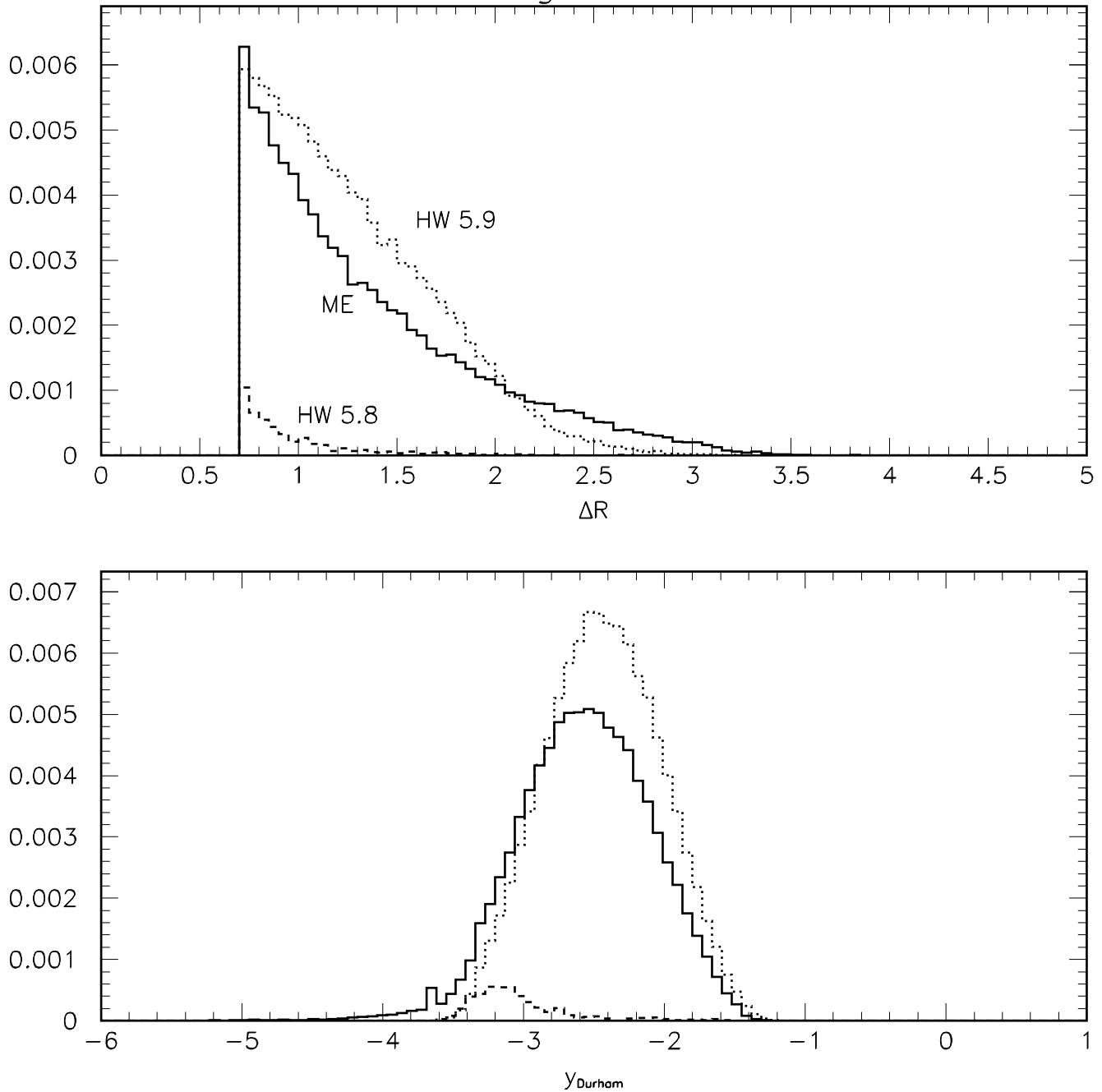


Figure 7: Distributions in (a) the minimum jet-jet angular separation  $\Delta R$  and (b) the minimum  $y$  among jet pairs (defined in the Durham algorithm) for additional jets produced in top production and decay in  $e^+e^-$  collisions at  $\sqrt{s} = 360$  GeV. Results are shown for the exact calculation (solid histogram, labeled ME) and as obtained using HERWIG version 5.8 (dotted histogram, labeled HW 5.8) and version 5.9 (dashed histogram, labeled HW 5.9).